Preprint No. 2019-01

Acquisition of polymorphic uncertain data based on computer tomographic scans and integration in numerical models of adhesive bonds

M. Drieschner*[1], Y. Petryna[1]

February 22, 2019

*Correspondence: M. Drieschner: martin.drieschner@tu-berlin.de
[1]Technische Universität Berlin, Faculty VI Planning Building Environment, Department of Civil Engineering, Chair of Structural Mechanics, Gustav-Meyer-Allee 25, 13355 Berlin, Germany

Suggested Citation: M. Drieschner, Y. Petryna. Acquisition of polymorphic uncertain data based on computer tomographic scans and integration in numerical models of adhesive bonds. *Preprint-Reihe des Fachgebiets Statik und Dynamik, Technische Universität Berlin*, Preprint No. 2019-01, 2019. http://dx.doi.org/10.14279/depositonce-8235.

Preprint-Reihe des Fachgebiets Statik und Dynamik, Technische Universität Berlin auf https:// depositonce.tu-berlin.de/

Acquisition of polymorphic uncertain data based on computer tomographic scans and integration in numerical models of adhesive bonds

M. Drieschner, Y. Petryna

Abstract

Since commercial wind turbines were introduced around 1980, the length of rotor blades has increased substantially up to 80m with consequently higher demands on availability and failure prevention. One of the typical failure mechanisms of rotor blades in operation are fatigue cracks in adhesive bonds often caused by air voids with a-priori unknown properties, which results from the manufacturing process. In this contribution, the usage of computer tomography as non-destructive testing (NDT) on a representative sub-component, called the Henkel beam, is proposed for air void detection and quantification. By using the NDT data, structural failure is simulated by means of a finite element approach under polymorphic uncertainties to consider diverse uncertainty sources in the data acquisition. On the one hand, aleatory irreducible uncertainties are described with stochastic variables and on the other hand, interval and fuzzy variables are used for epistemic reducible uncertainties. For solving the problem under polymorphic uncertainties, different computational methods within a MATLAB® framework called PolyUQ are used and compared with regard to accuracy and efficiency.

Keywords *data acquisition; aleatory and epistemic uncertainty; polymorphic uncertainty modeling; fuzzy-interval-stochastic finite element approach; structural failure quantification*

1 Introduction

This study has been performed within the research project MuScaBlaDes – "Multi-scale failure analysis with polymorphic uncertainties for optimal design of rotor blades" – which is part of the Priority Programme (SPP 1886) "Polymorphic uncertainty modelling for the numerical design of structures" started in 2016.

Rotor blades of wind turbines are thin-walled spatial structures consisting of two composite shells and a load-bearing structure inside. The latter one typically consists either of a box girder or spar caps integrated in the shells and one or two shear webs assembled with adhesive bonds. During the lifetime of wind turbines, the blades are stressed mainly by aerodynamic loads, but also by inertia, gravitational and gyroscopic loads which have to be taken into account in the design and certification process [4, 10]. Appearing extreme and fatigue loading can cause different failure mechanisms like delamination, buckling, cross-sectional distorsion and out-of-plane deformations at the root transition area. In a full-scale rotor blade test [22] according to [11], debonding of spar caps and shear webs has been identified as a significant reason for structural collapse. Inaccuracies and imperfections in manufacturing processes reduce the adhesive bond quality which affects the overall integrity and reliability of rotor blades.

In this regard, sub-components, e.g. the Henkel beam (HB) by the Fraunhofer Institute for Wind Energy and Energy System Technology (IWES), have been developed in the past for detailed experimental investigations [19, 23]. Of course, sub-components cannot be identical with

a certain part of the rotor blade, but at least representative with respect to loading, geometry, material, structural parameters, behavior and failure mechanisms, see section 2.

It could be seen that the fatigue damage mechanism is initiated by multiple cracks in the adhesive bonds due to air voids and debonding. For understanding the reasons of failure in detail, various NDT like ultrasonic (US) or computer tomographic (CT) scanning have been applied by *Technische Universität Berlin* within the collaborative research project "BladeTester - Automated approach for serial integrity tests of rotor blades of wind turbines" (2011-2015) [18]. In section 3, a-priori unknown air void properties in Henkel beams are classified and detected based on CT images in the data acquisition.

The obvious assumption that the crack initiation is probably caused by a critical stress concentration around the air void inclusions is analyzed by means of a finite element approach under polymorphic uncertainties. The processed air void properties (amount, shape, size and location) from the CT analysis are integrated in the numerical simulation. Randomness and natural variability as well as limited information, subjectivity and imprecise data lead to aleatory (*alea* (latin) = gambling, dice) and epistemic ($\epsilon\pi\iota\sigma\tau\acute{\eta}\mu\eta$ (greek) = science, profession) uncertainties, respectively [8, 16]. As an extension to probabilistic approaches [15, 21, 1, 13], the diversity of the uncertainty sources is considered, see [2] for an overview about possible models. In this study, stochastic, interval and fuzzy variables are used at once like in [20]. Different solution methods are compared with regard to accuracy and efficiency in a self-developed MATLAB® framework called PolyUQ, see section 4.

Finally, important from an engineering point of view, the numerical output for the relative bearing capacity of imperfect adhesive bonds is simplified before conclusions are given in section 5.

The main focus of this contribution is on the quantification of various structural parameters based on non-destructive testing and on the integration in numerical simulations of perforated structures by using polymorphic uncertainties, see also Fig. 1.

2 Adhesive bonds in a representative sub-component

2.1 Henkel beam as representative sub-component

For certification of a series of structurally identical rotor blades, static and cyclic full-scale tests on only one or maximum two rotor blades are required [11]. A drawback beside the high costs is that the test blades can only be representative due to the uniqueness of each one and due to the more complex environmental conditions in operation. Furthermore, the structural collapse is caused by local failure, therefore testing structural details is defined in international standards as [11]. With regard to adhesive bonds, mechanical tests at coupon level with thicknesses of $t = 0.5$mm and $t = 3.0$mm are required for material certification even though that is not realistic for practical rotor blade design [19, 23]. To close the gap between full-scale and coupon tests, the Fraunhofer IWES has developed the Henkel beam as a representative sub-component for detailed investigations on adhesive bonds, see Fig. 2.

The Henkel beam is fixed on the left and loaded vertically on the right. The definition of the loading is based on a stress state in the adhesive bonds in a full-scale test at a distance of 10m from blade root. For the underlying combined flap and edge wise static load case, the dominating stress σ_{11} is in length direction of the blade, whereas transerve and shear loading also exist up to 10% of σ_{11}.

The Henkel beam is constructed as a double T-girder following the cross-section of the load bearing structure in rotor blades, see Fig. 2a. In longitudinal direction, the beam is tapered so that the maximum stresses are located between the reinforcements, away from loading and fixation regions, to get failure cracks and structural collapse. Then, different designs and materials of adhesive bonds are investigated numerically as well as experimentally to understand the structural behavior.

Figure 1: Application-related strategy for data handling and integration in numerical uncertainty models

2.2 Properties of the adhesive bonds

The geometry, loading and material parameters of the adhesive bond in Fig. 3 are defined as described below according to Fig. 2b and Fig. 2c, respectively.

2.2.1 Geometry

Between the reinforcements on the edge regions of the Henkel beam, the region of interest has a length of $l = 700$mm in x-direction. Furthermore, the cross-section is defined with a width of $b = 32$mm in y-direction and a thickness of $t = 10$mm in z-direction. To avoid time-consuming numerical simulations, the resulting three-dimensional cuboid is simplified to a rectangular two-dimensional plate with constant thickness in section 4.

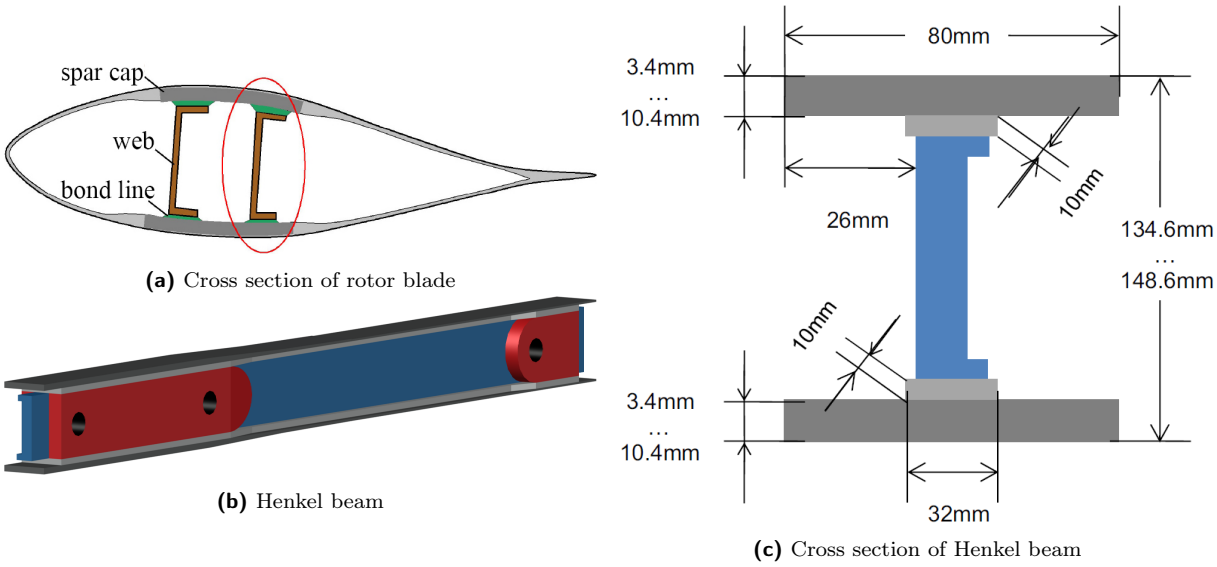

(a) Cross section of rotor blade

(b) Henkel beam

(c) Cross section of Henkel beam

Figure 2: Henkel beam geometry and relation to rotor blade according to [19]

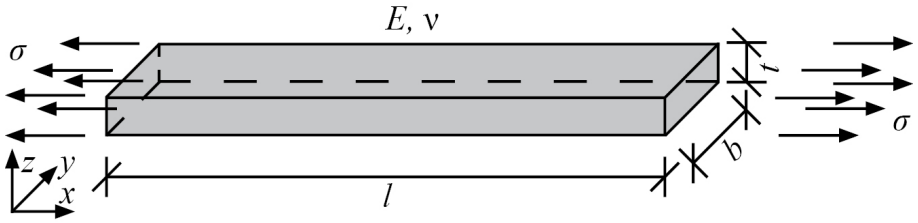

Figure 3: Adhesive bond under uniaxial tension

2.2.2 Loading

The Henkel beam is fixed on the left and loaded on the right in z-direction. Due to elastic behavior and present geometrical dimensions, the beam theory is valid so that a static loading of the Henkel beam leads to a linear strain distribution over the beam height. Consequently, the stress distribution over the adhesive bonds can be considered as constant caused by the relatively small thickness compared to the beam height.

2.2.3 Material

The adhesive bonds are made of epoxy resin, an isotropic material with Young's modulus $E = 4890\text{MPa}$ and Poisson's ratio $\nu = 0.22$. It is assumed a linear elastic material behavior until the first cracking that means local failure. It corresponds to a brittle behavior which is typical under fatigue loading of adhesive bonds. In addition, present air voids lead to an inhomogeneous structure, see section 3.

3 Computer tomographic scans

3.1 Data acquisition

In cooperation with the Fraunhofer IWES, ten Henkel beams have been used for various studies of adhesive bonds within the BladeTester project [18]. NDT have been applied before and after fatigue tests on several Henkel beams, see [14] for more details. Three of them - namely HB3, HB9 and HB10 - have been scanned with CT devices to detect and analyze the air voids in adhesive bonds. The quality of information depends obviously on the resolution, given as 3mm

in longitudinal direction and as approximately 296×182px in cross-sectional images. Due to the quasi-continuous measurement, air voids with a length lower than 3mm between two scans cannot be detected. Furthermore, detected air voids in the cross-sectional images are represented by discrete pixels.

On this basis the following procedure for data acquisition is implemented in MATLAB®, partly using the Image Processing Toolbox:

1. detection of the region of interest with a length of $l = 700$mm, as described in section 2
2. for all relevant two-dimensional CT images
   (a) import of the RGB image
   (b) converting in a gray image
   (c) detection of the two adhesive bonds in the Henkel beam
   (d) for all adhesive bonds
      i. image binarization
      ii. analysis of the air void properties (amount, shape, size and location)
      iii. calculation of the air voids content $\phi_{h,a}$ with $h \in \{3, 9, 10\}$ and $a \in \{1, 2\}$

All steps are based on subjective settings which influence the calculated air void properties and lead to an uncertain data acquisition.

Initially, each pixel holds three values

$$R \times G \times B \in [0, 255] \times [0, 255] \times [0, 255]\,, \tag{1}$$

depending on brightness (window level WL) and contrast (window width WW), see Fig. 4. With regard to the requirement that the adhesive bonds and the air voids have to be distinguishable in every cross-sectional image, the values WL = 800 and WW = 2500 have been chosen. For

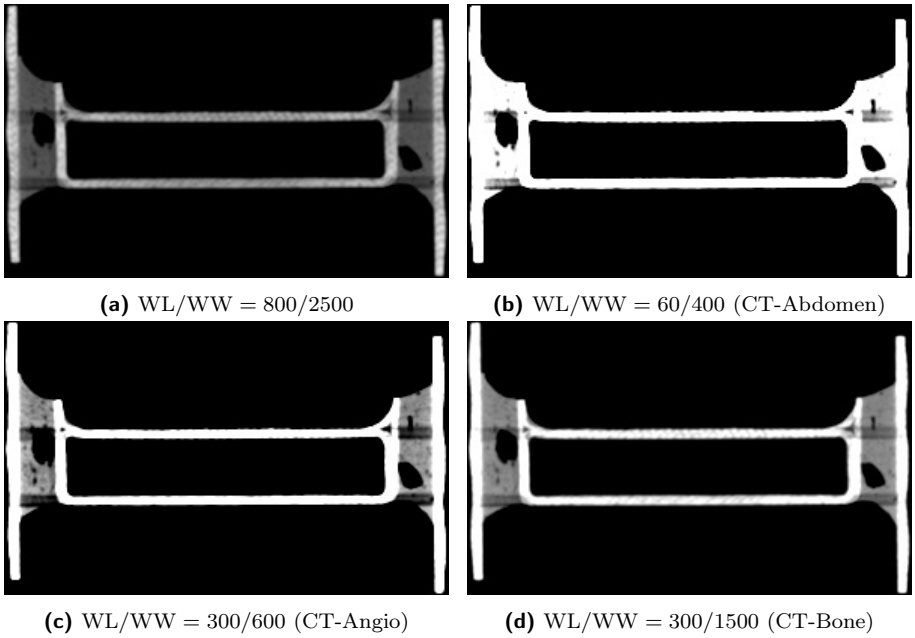

(a) WL/WW = 800/2500 **(b)** WL/WW = 60/400 (CT-Abdomen)

(c) WL/WW = 300/600 (CT-Angio) **(d)** WL/WW = 300/1500 (CT-Bone)

Figure 4: Chosen (a) and other possible (b-d) settings for brightness WL and contrast WW

comparing pixels to detect the adhesive bonds automatically, the RGB values are converted in a gray value using the following equation

$$Y = (0.2989R + 0.5870G + 0.1140B) \in [0, 255]\,. \tag{2}$$

The coefficients in Eq. (2) are equivalent to those used to calculate luminance E'_{Y} from the gamma pre-corrected primary analogue signals E'_{R}, E'_{G} and E'_{B} [5].

To decide whether a pixel belongs either to epoxy resin or to air voids, the gray images have to be binarized for which either Otsu's method [17] with a globally defined threshold or Bradley's method [3] with a locally adaptive threshold are common. In Fig. 5 the binarized images of the two adhesive bonds from Fig. 4a are shown depending on the method and the sensitivity factor or the global threshold, respectively. Representative studies have shown satisfactory results for

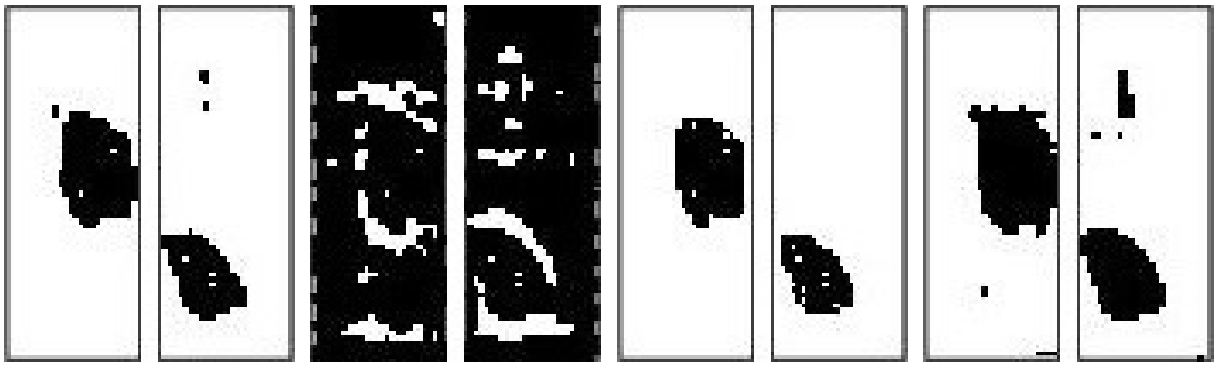

(a) Bradley's method sensitivity = 1.00 **(b)** Bradley's method sensitivity = 0.50 **(c)** Otsu's method threshold = 0.00 **(d)** Otsu's method threshold = 0.18

Figure 5: Chosen (a) and other possible (b-d) methods for image binarization

Bradley's method with highest sensitivity factor of 1.0 which is used for the data acquisition.

In this study, the air void properties of each CT image are smeared to define an air voids content over the region of interest in longitudinal direction for each Henkel beam h and each adhesive bond a:

$$\begin{aligned} \phi_{h,a}\colon\ [0,l] \subset \mathbb{R} &\to [0,1] \subset \mathbb{R} \\ x &\mapsto \phi_{h,a}(x) \qquad \forall h \in \{3,9,10\} \text{ and } a \in \{1,2\} \end{aligned} \tag{3}$$

3.2 Data processing

For integrating the acquired information of air voids into the numerical simulations of adhesive bonds, it is useful to simplify the air voids content $\phi_{h,a}$. Based on the assumption that air voids with large sizes influence the structural behavior more than air voids with small sizes, all those with a content less than 5% are neglected, so that

$$\phi_{h,a} = \begin{cases} \phi_{h,a}, & \text{if } \phi_{h,a} \geq 0.05 \\ 0, & \text{otherwise.} \end{cases} \tag{4}$$

In addition, the detected arbitrary air void shapes have to be parameterized. Therefore, the shape is simplified to a (slotted) hole, see Fig. 6. Each air void is defined about the location $(x_{\mathrm{M}}, y_{\mathrm{M}})$, the length l_{LP} in x-direction, the width b_{LP} in y-direction and the rotation $\alpha_{\mathrm{LP}} = 0°$ in x-y-plane. The red line in Fig. 7 describes the numerical approximation of the blue line based on the data processing for adhesive bond 1 of Henkel beam 10.

4 Polymorphic uncertainty modeling of adhesive bonds

4.1 Consideration of polymorphic uncertainties

The acquired and processed data on air void properties in adhesive bonds are integrated in structural failure simulations. Besides deterministic parameters, different uncertainty types based

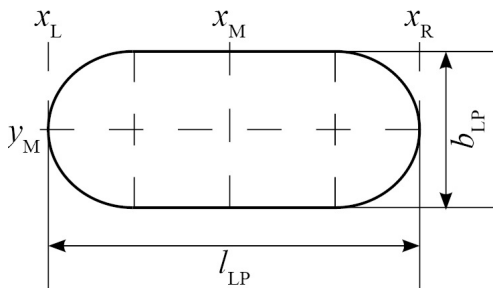

Figure 6: Slotted hole as simplified air void shape

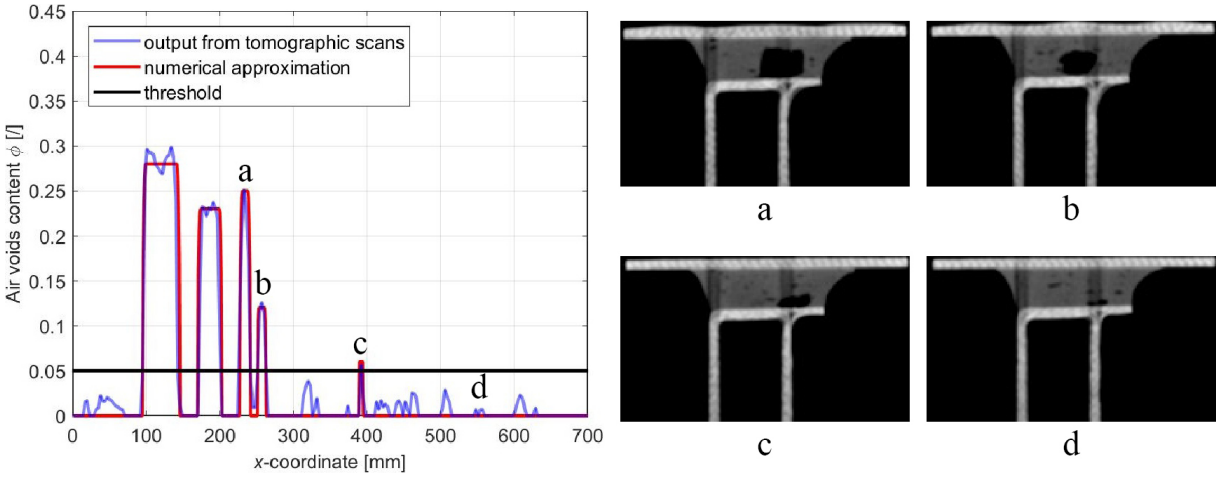

Figure 7: Exemplary air voids content $\phi_{10,1}$

Table 1: Input variables for adhesive bond simulations

name	unit	type	values
plate length	[mm]	deterministic	$l =$ 700
plate width	[mm]	deterministic	$b =$ 32
plate thickness	[mm]	deterministic	$t =$ 10
Young's modulus	[MPa]	deterministic	$E =$ 4890
Poisson's ratio	[/]	deterministic	$\nu =$ 0.22
uniaxial loading	[N]	deterministic	$F =$ 1
numerical parameter	[mm]	deterministic	$\epsilon =$ 0.5
amount of air voids	[/]	fuzzy	$n_{LP} =$ TFI $\langle 0, 2, 4, 6\rangle$
i-th air voids content	[/]	interval	$\phi_{LPi} =$ $[0.05, 0.40]$
i-th air voids size ratio	[/]	interval	$v_{LPi} =$ $[1.00, 7.00]$
midpoint x-location of air void i	[mm]	stochastic	$x_{Mi} \sim \mathcal{U}(a_{xi}, b_{xi})$
midpoint y-location of air void i	[mm]	stochastic	$y_{Mi} \sim \mathcal{U}(a_{yi}, b_{yi})$

on different uncertainty sources are considered, see Table 1. Expert knowledge on a limited amount of six adhesive bonds can be taken into account, so that the amount of air voids n_{LP} is quantified by a trapezoidal fuzzy interval (TFI) with a support $S_{n_{\mathrm{LP}}} = [0, 6]$ and a core $C_{n_{\mathrm{LP}}} = [2, 4]$. The membership function $\mu(n_{\mathrm{LP}})$ is discrete because the amount of air voids is naturally represented by a positive integer.

Various subjective settings in the CT image analysis affect mainly the size of air voids for which no expert knowledge is available. As a result the air voids content $\phi_{\mathrm{LP}i}$ and the air voids size ratio $v_{\mathrm{LP}i}$ are defined as interval variables from which the width $b_{\mathrm{LP}i} = \phi_{\mathrm{LP}i} b$ and the length $l_{\mathrm{LP}i} = v_{\mathrm{LP}i} b_{\mathrm{LP}i}$ can be calculated, respectively.

Additionally, natural variability and randomness of the air void location lead to aleatory uncertainties which are described with stochastic variables $x_{\mathrm{M}i}$ and $y_{\mathrm{M}i}$. The bounds of the uniform distribution for $x_{\mathrm{M}i}$ are calculated for each air void $i = \{1, \ldots, n_{\mathrm{LP}}\}$ as follows: An effective length $l_{\mathrm{eff}} = l - 2b$ is divided in equidistant subdomains with a length of $l_i = l_{\mathrm{eff}}/n_{\mathrm{LP}}$ and bounds $[x_{\min,i}, x_{\max,i}] = [b + (i-1)l_i, b + il_i]$ in x-direction. To avoid numerical problems, the equation $x_{\min,i} + \epsilon \leq x_{\mathrm{L}i} < x_{\mathrm{R}i} \leq x_{\max,i} - \epsilon$ has to be valid for each air void. The relation $x_{\mathrm{M}i} = (x_{\mathrm{L}i} + x_{\mathrm{R}i})/2$ leads to

$$\begin{array}{rcll} a_{\mathrm{x}i} & = & x_{\min,i} + \epsilon + \frac{l_{\mathrm{LP}i}}{2} = b + (i-1)\frac{l-2b}{n_{\mathrm{LP}}} + \epsilon + \frac{v_{\mathrm{LP}i}\phi_{\mathrm{LP}i}b}{2} & \text{and} \\ b_{\mathrm{x}i} & = & x_{\max,i} - \epsilon - \frac{l_{\mathrm{LP}i}}{2} = b + i\frac{l-2b}{n_{\mathrm{LP}}} - \epsilon - \frac{v_{\mathrm{LP}i}\phi_{\mathrm{LP}i}b}{2}. & \end{array} \tag{5}$$

For the bounds of the uniform distribution for $y_{\mathrm{M}i}$, one obtains

$$\begin{array}{rcll} a_{\mathrm{y}i} & = & \frac{b_{\mathrm{LP}i}}{2} = \frac{\phi_{\mathrm{LP}i}b}{2} & \text{and} \\ b_{\mathrm{y}i} & = & b - \frac{b_{\mathrm{LP}i}}{2} = b - \frac{\phi_{\mathrm{LP}i}b}{2}. & \end{array} \tag{6}$$

The Eq. (5) and (6) ensure, on the one hand, that each air void is completely inside the plate and, on the other hand, that no overlapping is occurred.

In conclusion, the vector

$$\begin{array}{rcl} \boldsymbol{\xi} & = & [\xi_{\mathrm{F}}, \boldsymbol{\xi}_{\mathrm{I}}, \boldsymbol{\xi}_{\mathrm{S}}] \\ & = & [n_{\mathrm{LP}}, \phi_{\mathrm{LP}1}, v_{\mathrm{LP}1}, x_{\mathrm{M}1}, y_{\mathrm{M}1}, \ldots, \phi_{\mathrm{LP}n_{\mathrm{LP}}}, v_{\mathrm{LP}n_{\mathrm{LP}}}, x_{\mathrm{M}n_{\mathrm{LP}}}, y_{\mathrm{M}n_{\mathrm{LP}}}] \end{array} \tag{7}$$

collects all fuzzy (ξ_{F}), interval ($\boldsymbol{\xi}_{\mathrm{I}}$) and stochastic ($\boldsymbol{\xi}_{\mathrm{S}}$) uncertain parameters which require an analysis under polymorphic uncertainties. The length of $\boldsymbol{\xi}$ corresponds to the total number of uncertain input variables which is itself uncertain.

4.2 Solving

4.2.1 Uncertainty handling

A MATLAB® framework called PolyUQ has been developed inhouse for solving problems under polymorphic uncertainties, also with an integrated interface to black-box solvers, see Fig. 8. In addition to the deterministic model, all uncertain variables and the described parametric dependencies,

- the reduced transformation method with three α levels for the fuzzy variable [9],
- the vertex method for the interval variables [7] and
- the Monte Carlo sampling as well as the Latin hypercube sampling with $n = 10^3$ simulations in each fuzzy-interval configuration for the stochastic variables [21]

have been selected as solution methods, see also Fig. 9.

In the fuzzy space, all possible values for n_{LP} except $n_{\mathrm{LP}} = 3$ are used. Monotonic behavior of the solution with regard to the amount of air voids is expected so that the evaluation of

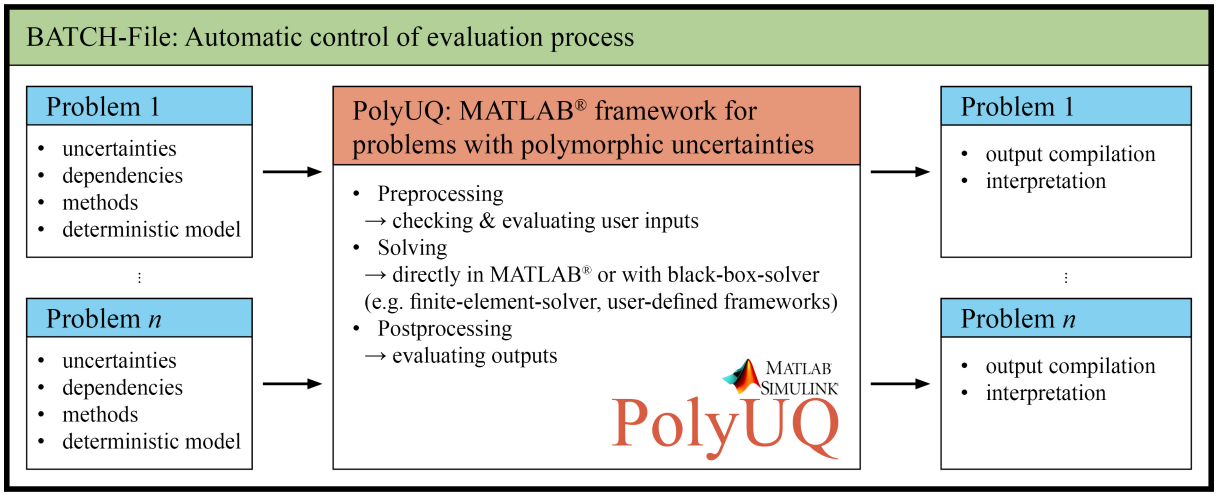

Figure 8: PolyUQ

$n_{\mathrm{LP}} = 2$ and $n_{\mathrm{LP}} = 4$ results in the correct solution on the core. Also monotony is presumed in the interval space which leads to the vertex method as reasonable method. For the stochastic space, the Latin hypercube sampling is implemented besides the classical Monte Carlo sampling. An integration of quasi-random point sets or stochastic collocation methods for comparison is going beyond the scope of the present study.

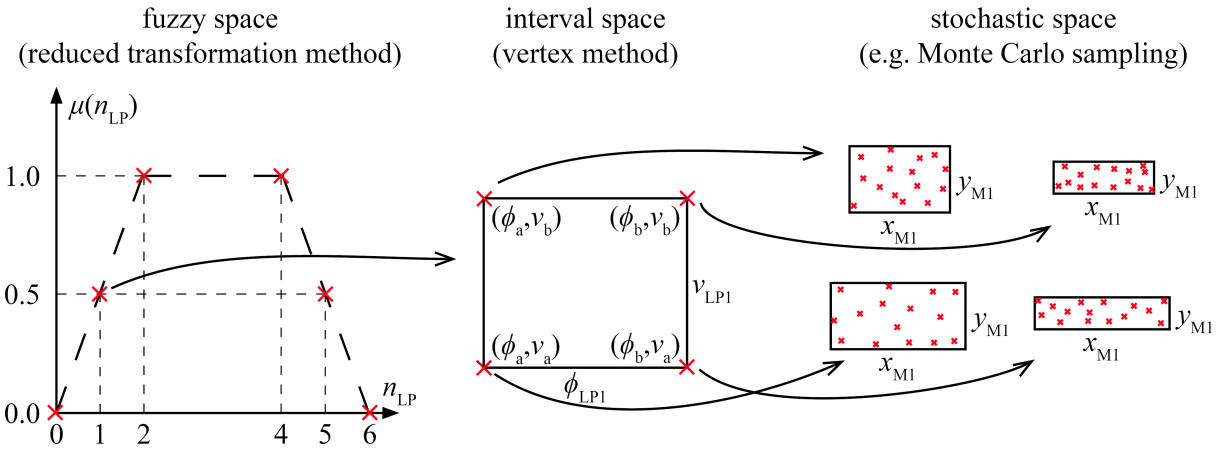

Figure 9: Solution strategy for problem under polymorphic uncertainties

4.2.2 Numerical model

For each fuzzy-interval-stochastic sample the linear elastostatic boundary value problem without body forces

$$
\begin{aligned}
\mathbf{0} &= \operatorname{div}\boldsymbol{\sigma} && \text{equilibrium equation in } D \\
\boldsymbol{\epsilon} &= \left[\nabla\boldsymbol{u} + \nabla^{\mathrm{T}}\boldsymbol{u}\right]/2 && \text{strain-displacement equation in } D \\
\boldsymbol{\sigma} &= \boldsymbol{C} : \boldsymbol{\epsilon} && \text{constitutive equation in } D \\
\boldsymbol{u} &= \mathbf{0} && \text{Dirichlet boundary conditions on } \Gamma_{\mathrm{u}} \\
\boldsymbol{\sigma}\cdot\boldsymbol{n} &= (\sigma_{\mathrm{ideal}}, 0)^{\mathrm{T}} && \text{Neumann boundary conditions on } \Gamma_{\sigma} \\
\boldsymbol{\sigma}\cdot\boldsymbol{n} &= \mathbf{0} && \text{Neumann boundary conditions on } \Gamma_{\sigma,0}
\end{aligned}
\tag{8}
$$

is solved within a finite element simulation. The two-dimensional plate under plane stress is fixed at one edge $\Gamma_{\mathrm{u}}(x = 0\mathrm{mm})$ and uniformly loaded in x-direction at another edge

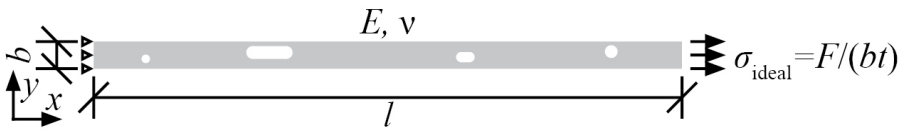

Figure 10: Numerical adhesive bond model

$\Gamma_\sigma(x = l = 700\text{mm})$, see Fig. 10. Isotropic material with linear elastic behavior is defined. The structure is meshed by two-dimensional 8-node elements with quadratic displacement behavior whereby the air voids are cut out and not meshed. The amount of nodes and elements depends on all uncertain parameters $\boldsymbol{\xi}$ due to mesh refinement around each air void. From the resulting displacement vector $\boldsymbol{u}$, the stress field $\boldsymbol{\sigma}(\boldsymbol{u})[\boldsymbol{x}]$ can be calculated. The crack initiation is located on the point of maximum first principal stress in the structure which is determined by

$$\sigma_{\max} = \operatorname*{ess\,sup}_{\boldsymbol{x}\in D} \lambda_{\max}(\boldsymbol{\sigma}(\boldsymbol{u})[\boldsymbol{x}])\,. \tag{9}$$

Here $\lambda_{\max}$ denotes the largest eigenvalue of $\boldsymbol{\sigma}$. As quantity of interest, a relative bearing capacity

$$\frac{F_{\max}}{F_{\text{ideal}}} = \frac{\sigma_{\text{ideal}}}{\sigma_{\max}} = \frac{F/(bt)}{\sigma_{\max}} \in [0\%, 100\%] \tag{10}$$

is defined to quantify the influence of air voids on structural failure.

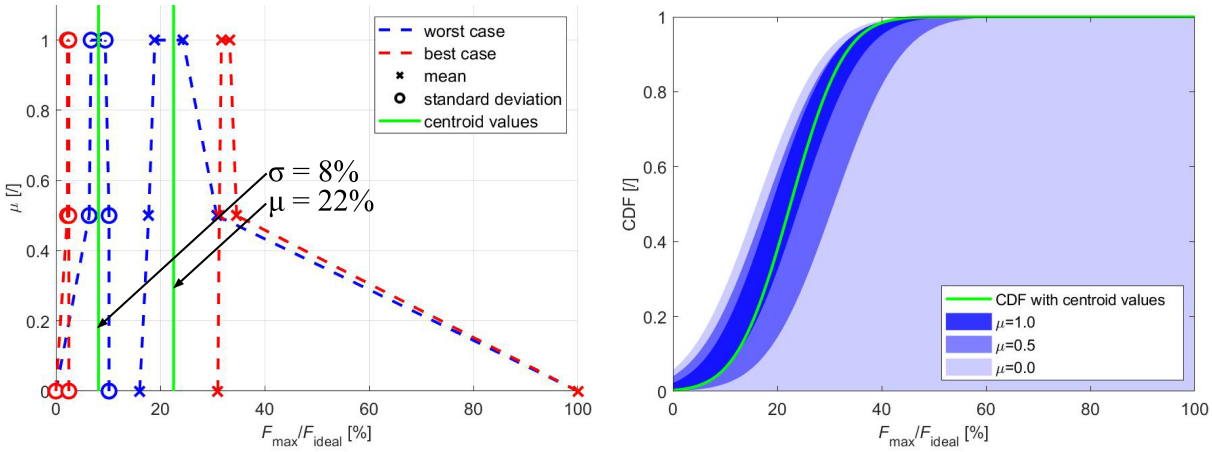

(a) Membership functions

(b) Cumulative distribution functions

Figure 11: Fuzzy-interval-stochastic output and corresponding defuzzification

4.3 Results

The quantity of interest $F_{\max}/F_{\text{ideal}} = F_{\max}/F_{\text{ideal}}\,(\xi_{\text{F}}, \boldsymbol{\xi}_{\text{I}}, \boldsymbol{\xi}_{\text{S}})$ is polymorphic uncertain since it depends on all uncertain parameters. Important from an engineering point of view is to generate a simplified and practicable output as follows:

1. calculate the mean and standard deviation in stochastic space
   $F_{\max}/F_{\text{ideal}}\,(\xi_{\text{F}}, \boldsymbol{\xi}_{\text{I}}, \boldsymbol{\xi}_{\text{S}}) \rightarrow \mu_{F_{\max}/F_{\text{ideal}}}\,(\xi_{\text{F}}, \boldsymbol{\xi}_{\text{I}})$ and $\sigma_{F_{\max}/F_{\text{ideal}}}\,(\xi_{\text{F}}, \boldsymbol{\xi}_{\text{I}})$

2. calculate the lower and upper bounds in interval space
   $\mu_{F_{\max}/F_{\text{ideal}}}\,(\xi_{\text{F}}, \boldsymbol{\xi}_{\text{I}}) \rightarrow \left[\mu_{\min,F_{\max}/F_{\text{ideal}}}\,(\xi_{\text{F}}), \mu_{\max,F_{\max}/F_{\text{ideal}}}\,(\xi_{\text{F}})\right]$
   $\sigma_{F_{\max}/F_{\text{ideal}}}\,(\xi_{\text{F}}, \boldsymbol{\xi}_{\text{I}}) \rightarrow \left[\sigma_{\min,F_{\max}/F_{\text{ideal}}}\,(\xi_{\text{F}}), \sigma_{\max,F_{\max}/F_{\text{ideal}}}\,(\xi_{\text{F}})\right]$

3. calculate the discrete membership functions in fuzzy space
   $\mu_{\min,F_{\max}/F_{\text{ideal}}}(\xi_{\text{F}}) \rightarrow \mu\left(\mu_{\min,F_{\max}/F_{\text{ideal}}}\right)$
   $\mu_{\max,F_{\max}/F_{\text{ideal}}}(\xi_{\text{F}}) \rightarrow \mu\left(\mu_{\max,F_{\max}/F_{\text{ideal}}}\right)$
   $\sigma_{\min,F_{\max}/F_{\text{ideal}}}(\xi_{\text{F}}) \rightarrow \mu\left(\sigma_{\min,F_{\max}/F_{\text{ideal}}}\right)$
   $\sigma_{\max,F_{\max}/F_{\text{ideal}}}(\xi_{\text{F}}) \rightarrow \mu\left(\sigma_{\max,F_{\max}/F_{\text{ideal}}}\right)$

4. defuzzify the discrete worst case membership functions (minimum mean with maximum standard deviation) by the centroid method (e.g. described in [16]), see Fig. 11a

5. visualize the worst case fuzzy and defuzzied cumulative distributive functions (CDF) for plausibility check, see Fig. 11b

A defuzzified worst case mean value of $\mu_{F_{\max}/F_{\text{ideal}}} = 22\%$ and a defuzzified worst case standard deviation of $\sigma_{F_{\max}/F_{\text{ideal}}} = 8\%$ have been calculated. This means that adhesive bonds with air voids show a considerably smaller bearing capacity in comparison with an adhesive bond free of air voids. Fig. 12 underlines a satisfactory accuracy with regard to the number of simulations in the stochastic space. Comparing the efficiency of Monte Carlo sampling and Latin hypercube sampling, no significant difference can be detected, see also [6]. With regard to the theoretical

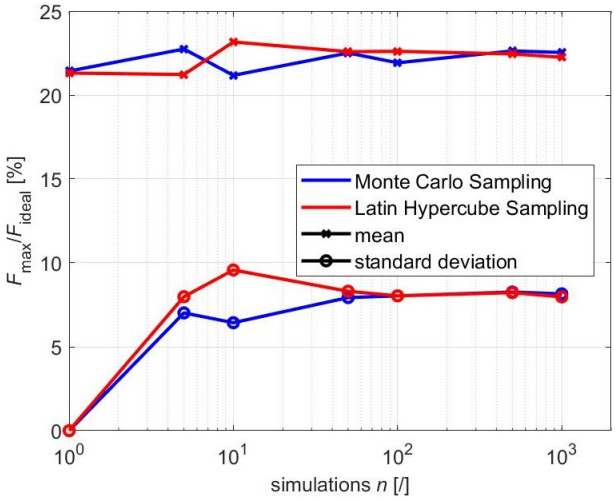

Figure 12: Convergence of defuzzied worst case parameters

solution [12] of the relative bearing capacity $F_{\max}/F_{\text{ideal}} = 33\%$ for an infinite plate with one circular hole, the influence of finite plate dimensions as well as of higher amount of air voids has been quantified in this study.

5 Conclusions

An important component in the load-bearing structure of rotor blades of wind turbines are adhesive bonds which are in the focus of this contribution. A numerical model for investigations of air void impacts on structural failure has been presented. The air void properties are based on experimental data obtained by computer tomographic scans on a representative sub-component. Diverse uncertainties have been presented in the data acquisition and data processing which have been divided into epistemic and aleatory ones, respectively, thus lead to a problem under polymorphic uncertainties. On this basis, fuzzy, interval and stochastic variables have to be taken into account for uncertainty quantification and integration in numerical simulations. The relative bearing capacity as quantity of interest has been evaluated on a two-dimensional plate under plane stress loaded by uniaxial tension. Different applied solution methods have been compared with regard to accuracy as well as efficiency and have shown similar results. It has

been determined that the mutual influence between air voids as well as the influence of the finite plate dimensions reduce considerably the bearing capacity of adhesive bonds. The output including polymorphic uncertainties provides the possibility to analyze the impact of different uncertainty sources on the result.

6 Future work

The authors are currently working on the extension to multi-scale models, on the consideration of arbitrary air void shapes and on more efficient methods for solving problems under polymorphic uncertainties. Also the validation of numerical structural failure simulations with experiments is an ongoing work and will be presented in future.

Acknowledgement

The authors gratefully acknowledge the financial support of the German Research Foundation (DFG) within the Priority Programme "Polymorphic uncertainty modelling for the numerical design of structures – SPP 1886".

The contribution was enriched by helpful discussions with our colleagues Dietmar Hömberg, Martin Eigel and Robert Gruhlke from *Weierstraß-Institut für Angewandte Analysis und Stochastik (WIAS) Berlin* within our collaborative project "MuScaBlaDes: Multi-scale failure analysis with polymorphic uncertainties for optimal design of rotor blades".

References

[1] K. C. Bacharoudis and T. P. Philippidis. A probabilistic approach for strength and stability evaluation of wind turbine rotor blades in ultimate loading. *Structural Safety*, 40:31–38, 2013.

[2] M. Beer, S. Ferson, and V. Kreinovich. Imprecise probabilities in engineering analyses. *Mechanical Systems and Signal Processing*, 37:4–29, 2013.

[3] D. Bradley and G. Roth. Adaptive thresholding using the integral image. *Journal of Graphics Tools*, 12(2):13–21, 2007.

[4] P. Brøndsted and R. P. L. Nijssen, editors. *Advances in wind turbine blade design and materials*. Woodhead Publishing Series in Energy, 2013.

[5] CCIR: Comité Consultatif International des Radiocommunications. Studio encoding parameters of digital television for standard 4:3 and wide screen 16:9 aspect ratios (ITU-R BT.601-7:2011), March 2011.

[6] L. Chrisman. Latin Hypercube vs. Monte Carlo Sampling, 2014. http://www.lumina.com/blog/latin-hypercube-vs.-monte-carlo-sampling; retrieved September 20, 2018.

[7] W. Dong and H. C. Shah. Vertex method for computing functions of variables. *Fuzzy Sets and Systems*, 24:65–78, 1987.

[8] W. Graf, M. Götz, and M. Kaliske. Analysis of dynamical processes under consideration of polymorphic uncertainty. *Structural Safety*, 52:194–201, 2015.

[9] M. Hanss. *Applied Fuzzy Arithmetic - An Introduction with Engineering Applications*. Springer, 2005.

[10] IEC: International Electrotechnical Commission. Wind turbines - Part 1: Design requirements (IEC 61400-1:2005), August 2005.

[11] IEC: International Electrotechnical Commission. Wind turbines - Part 23: Full-scale structural testing of rotor blades (IEC 61400-23:2014), April 2014.

[12] E. Kirsch. Die Theorie der Elastizität und die Bedürfnisse der Festigkeitslehre. *Zeitschrift des Vereines deutscher Ingenieure*, 42:797–807, 1898.

[13] D. Kovačević, Y. Petryna, and M. Petronijević. Assessment of the impact of air voids on adhesive joints in rotor blades by use of NDT and FEA. *EWSHM 2016*, 2016.

[14] A. Künzel. *Parameteridentifikation auf Basis faseroptisch gemessener quasi-kontinuierlicher Dehnungssignale*. PhD thesis, Techische Universität Berlin, 2016.

[15] O. P. LeMaître and O. M. Knio. *Spectral Methods for Uncertainty Quantification*. Springer, 2010.

[16] B. Möller and M. Beer. *Fuzzy Randomness - Uncertainty in Civil Engineering and Computational Mechanics*. Springer, 2004.

[17] N. Otsu. A threshold selection method from gray-level histograms. *IEEE Transactions on Systems, Man, and Cybernetics*, 9(1):62–66, 1979.

[18] Y. Petryna. Automatisiertes Verfahren für serienmäßige Integritätsprüfung von Rotorblättern und Bereitstellung von Rotorblatt-Tunern - Abschlussbericht. Technical report, TU Berlin, BAM - Bundesanstalt für Materialforschung und -prüfung and Steinbichler Optotechnik GmbH, 2015.

[19] F. Sayer, A. Antoniou, and A. van Wingerde. Investigation of structural bond lines in wind turbine blades by sub-component tests. *Adhesion and Adhesives*, 37:129–135, 2012.

[20] C. Wang and Z. Qiu. Hybrid uncertain analysis for temperature field prediction with random, fuzzy and interval parameters. *International Journal of Thermal Sciences*, 98:124–134, 2015.

[21] D. Xiu. *Numerical Methods for Stochastic Computation*. Princeton University Press, 2010.

[22] J. Yang, C. Peng, J. Xiao, J. Zeng, S. Xing, J. Jin, and H. Deng. Structural investigation of composite wind turbine blade considering structural collapse in full-scale static tests. *Composite Structures*, 97:15–29, 2013.

[23] D. S. Zarouchas, A. A. Makris, F. Sayer, D. V. Hemelrijck, and A. M. V. Wingerde. Investigations on the mechanical behavior of a wind rotor blade subcomponent. *Composites: Part B*, 43:647–654, 2012.